SAND99-1068J

Nucleation and Growth of GaN on GaAs (001) Substrates

Timothy J. Drummond, Michael J. Hafich, Stephen R. Lee,

John P. Sullivan, and Edwin J. Heller

Sandia National Laboratories

Albuquerque, NM 87185

Sergei Ruvimov and Zuzanna Liliental-Weber

Lawrence Berkeley Laboratory

Berkeley, CA 94720

Abstract

The nucleation of GaN thin films on GaAs is investigated for growth at 620 °C. An rf plasma cell is used to generate chemically active nitrogen from N_2. An arsenic flux is used in the first eight monolayers of nitride growth to enhance nucleation of the cubic phase. Subsequent growth does not require an As flux to preserve the cubic phase. The nucleation of smooth interfaces and GaN films with low stacking fault densities is dependent upon relative concentrations of active nitrogen species in the plasma and on the nitrogen to gallium flux ratio.

Introduction

To achieve the growth of single crystal epitaxial of GaN on GaAs two issues must be addressed. First, GaN and GaAs have different crystal structures. GaN forms in the hexagonal wurtzite structure ($P6_3mc$) while GaAs forms in the cubic zincblende structure ($F\bar{4}3m$). However, both crystals are based on tetrahedrally bonded units and differ only in the stacking sequence along the (0001) hexagonal/(111) cubic axis. It is well known that a cubic substrate template can promote the nucleation of a metastable cubic nitride thin film. This has been demonstrated for GaN growth on cubic substrates such as Si, GaAs, SiC and MgO. One reason to expect the promotion of the cubic phase is that it is geometrically impossible to fully relieve the lattice misfit stress between a (001) cubic surface and a well defined low index plane in the wurtzite structure via an interfacial dislocation network.[1] This effect was predicted to be a strong driving force for the promotion of a cubic nitride overgrowth.

Second, GaN has a substantially smaller bond length than GaAs. The cubic GaN bond length is 0.1949 nm while the bond length of GaAs is 0.2448 nm at room temperature. This corresponds to a 20.4% mismatch in bond length with respect to GaAs. With this much mismatch not even a single monolayer of GaN can be supported on a GaAs substrate in the continuum elastic limit. Rather there is a critical island diameter of about five GaN molecules which can be formed on a GaAs surface before the onset of dislocation formation. This suggests the possibility of creating a fully relaxed

DISCLAIMER

Portions of this document may be illegible in electronic image products. Images are produced from the best available original document.

GaN overlayer on a GaAs substrate. The misfit could be accommodated by a square grid of edge dislocations established during the growth of the first one to two monolayers of GaN.

A fundamental assumption to be satisfied for the process to work was that it would be possible, in an ultrahigh vacuum environment, to synthesize a GaN surface monolayer on a GaAs substrate via a N → As replacement reaction. The reaction of GaAs with P or Sb fluxes can be tailored to yield smooth atomically abrupt interfaces.[2-5] In the case of binary heterojunctions of GaSb or InSb on GaAs relaxation is accomplished by the formation of a square array of edge dislocations at the interface.[6-9] GaSb on GaAs has a mismatch 7.8% and the edge dislocation array is associated with two monolayer corrugation of the interface with a periodicity roughly equal to the dislocation spacing. For InSb on GaAs the misfit is 14.6% and the interfaces are not corrugated. Instead the interfaces are "rippled" with a fairly regular period of 40-50 nm and an amplitude of about 3 nm. The nonplanarity of the interfaces is driven by surface stress associated with the lattice mismatch between the two materials. The difference between finding corrugation and rippling is likely due to the fact that there is a finite critical layer thickness for dislocation formation for GaSb on GaAs while GaAs can support pseudomorphic InSb only as submonolayer islands which promotes the formation of the edge dislocation array.[9] If the reaction of nitrogen with a GaAs surface were limited to the first 1-2 monolayers then the 20.3%

mismatch between GaN and GaAs should result in the formation of a regular edge dislocation array with a relatively planar interface.

The first phase in this investigation was to investigate the reaction of ammonia with a GaAs substrate and with elemental Ga deposited on a GaAs substrate. No reaction was observed at temperatures up to 640 °C at which point the GaAs begins to decompose with the preferential evaporation of arsenic. Based on beam flux measurements it was found that a temperature of 690±1 °C was required to crack the ammonia in the gas injection cell. This is consistent with the fact that GaN could be readily grown at 700 °C with uncracked ammonia and elemental Ga.

During growth at 700 °C with ammonia, degradation of the GaAs/GaN interface was observed and only hexagonal GaN films were obtained. Transmission electron microscopy (TEM) investigations showed that Ga was being lost from the GaAs matrix leaving behind elemental As. To address this issue an rf plasma source was substituted for the ammonia source. The intent was to produce chemically active nitrogen from the plasma to allow growth at lower temperatures. After characterizing the plasma cell a GaAs/GaN nucleation study was performed varying both the nitrogen flow (for a fixed rf power) and the Ga flux to optimize the structural and electrical properties of the interface. An arsenic flux was employed during the growth of the first eight GaN monolayers to promote cubic phase nucleation. The observed trends suggest that both the nitrogen to gallium flux ratio and the relative concentration of nitrogen species in the plasma flux are important in

determining the quality of the interface and the stacking fault density in the GaN overgrowth.

Experimental Setup

Nucleation and growth experiments were performed in a RIBER 32P molecular beam epitaxy (MBE) system. GaN films 50-100 nm thick were deposited on 500 nm n^- ($2x10^{16}/cm^3$) GaAs:Sn epilayers grown on 200 nm n^+ GaAs:Sn epilayers to bury the interface with the n^+ GaAs substrate. Ga and Sn were evaporated from conventional effusion cells. As_4 was evaporated from a valved cracking cell with the cracking section held at 600 °C. Valving was used to obtain abrupt changes in the As flux. Active nitrogen was obtained using an Oxford Applied Research (OAR) MPD21R rf plasma source. The nitrogen was supplied from the boil-off of the clean room LN_2 supply and passed through a Nanochem™ purifilter prior to being sent to the plasma source.

All experiments were performed on nominally singular (001) n^+ GaAs substrates. The n^+/n^- epitaxial GaAs buffer layers were designed to allow the C-V and I-V characterization of the GaN/GaAs interface. The GaAs was always grown at 590 °C with As_4 using Sn as a dopant. The As_4/Ga beam equivalent pressure (BEP) ratio on an ion gauge in the growth position was 15:1. Upon completion of the GaAs buffer layer the Ga and Sn fluxes were stopped while the As_4 flux was left on. The Ga cell temperature was reset to that desired for the GaN growth and the substrate temperature was increased to 620 °C. When the Ga cell and substrate temperatures had stabilized, a nitrogen plasma was lit behind a closed shutter. Prior to lighting the plasma RHEED indicated an As rich (2 × 4) surface reconstruction. The nucleation

and growth experiments described in the present work were performed by opening the plasma shutter immediately after lighting and tuning the plasma cell.

At 620 °C under an As_4 flux, plasma activated nitrogen leaking around the closed shutter was found to create an intense (3 × 3) reconstruction which subsequently transformed into a (1 × 1) GaN pattern (nitrogen rich surface reconstruction) in a matter of 2 to 5 minutes. The (3 × 3) reconstruction was found to give rise to a 3 × reconstruction along the (100) azimuth as well as the two (110) azimuths. Attempts to control the transformation from the (3 × 3) to a streaky GaN pattern at 620 °C in a migration enhanced epitaxy mode alternately adding a monolayer of Ga and relighting the plasma source behind the closed shutter were unsuccessful.

The (3 × 3) reconstruction has been reported by several groups[10-15]. The real space structure giving rise to the reconstruction has been studied by scanning tunneling microscopy (STM)[14,15]. The structure has been proposed to arise from rows of nitrogen dimer pairs separated by single dimer vacancy rows. It has been noted that nitrogen dimers should be energetically unstable due to the small N-N bond length[16]. We suggest that the (3 × 3) structure is due to antiparallel As-N dimer pairs, i.e. a square As_2N_2 block separated by dimer vacancy rows. This would relax both bond length and charge transfer constraints. Further, As-N bonds are known to be stable on the GaAs(001) surface up to at least 450 °C in the absence of atomic hydrogen[17].

Experiments using plasma activated nitrogen were performed using an orifice plate on the plasma cell containing 37 holes 1 mm in diameter (referred to henceforth as the high conductance orifice). Unless otherwise specified, experiments were run with a rf power of 300 W delivered to the plasma. Lighting the plasma required an initial flow of 20 sccm of N_2. Upon lighting the plasma the N_2 flow was reduced to that desired for growth and the source was tuned to minimize reflected power. As soon as the plasma source was tuned the nitrogen shutter and the Ga shutter were opened manually. The nitrogen shutter was opened first followed as quickly as possible by the Ga shutter. The As_4 source was left on for approximately the first eight monolayers of GaN growth at which time it was valved off.

The nitrogen supply was initiated slightly before the Ga supply to avoid forming a Ga rich surface which is believed to promote the nucleation of the hexagonal phase. The presence of an As flux during the growth of GaN has also been reported to enhance the purity of the cubic phase during epitaxy using an rf plasma source although GaAs precipitates were often observed in βGaN grown under an As_2 flux at temperatures of less than 700 °C. [18] The intent here was to guarantee an As rich surface stoichiometry throughout the nucleation stage while minimizing the potential for GaAs precipitation during growth at 620 °C. Growth times for the GaN were intended to produce films either 80 or 100 nm thick. Due to the high density of nitrogen molecules/ions/atoms in the plasma stream substantial gas phase scattering of the Ga out of its normal beam path occurred.

To calibrate the Ga flux, RHEED oscillations of GaAs growth using the desired Ga flux were first performed in a vacuum. This gives a Ga flux related to the dimensions and temperature of the effusion cell. For this measurement the Ga mean free path in the vacuum system is much greater than the distance from the effusion cell to the substrate. The measurement was then repeated as a function of N_2 flow through the unlit plasma source. For growth in high background pressures kinetic theory implies that the effective metal flux, j_m, reaching the substrate should vary as

$$j_m = j_{m0}/(1+\pi\sigma LP/kT)$$

where j_{m0} is the metal flux reaching the substrate in a vacuum, σ is the molecular cross-section, L is the distance from the source to the substrate, P is the background pressure, and kT is the thermal energy of the metal beam. [11] In the present application the growth rate under a nitrogen flux, R_{N2}, was measured as a function of nitrogen flow into the plasma cell, Φ_{N2}. The data was fit to an expression of the form

$$R_{N2} = R_o/(1 + r\Phi_{N2})$$

where R_o is the growth rate in vacuum and r is a constant. The substitution of Φ_{N2} for P is based on the observed linear variation $P_{N2} = 0.0246\Phi_{N2}$. P_{N2} is the beam equivalent nitrogen pressure measured on an ion gauge in the growth position measured in mTorr and the Φ_{N2} is measured in sccm. For GaAs and InAs r = 0.0451, for AlAs r = 0.0922. The similarity between the GaAs and InAs values and the large disparity with the AlAs value suggest gas

phase reaction with the Al reduces the effective Al flux before it reaches the substrate. Based on ellipsometrically determined nitride layer thicknesses a further 10-20% reduction in the Ga flux results when a plasma stream replaces a cold N_2 stream at a fixed flow rate. The substitution of the plasma for the cold nitrogen increases the kinetic energy and reactivity of the nitrogen providing two paths for the increased Ga flux reduction.

Growth times for the GaN films were estimated from GaAs growth rates measured under flowing N_2. The GaAs growth rate was then converted to a GaN growth rate by scaling according to the relative atomic densities of the two crystals. The resulting rate is designated R_{N2}(GaN). In some experiments the effect of plasma related scattering was factored into the growth time calculation. This estimation of growth rate assumes (001) βGaN growth. Given that the densities of the two crystal structures are virtually identical the βGaN growth rate will be reasonably accurate for estimating the thickness of either single or mixed phase epitaxial films.

To evaluate the plasma composition at 300 W rf input power the optical emission spectrum of the nitrogen plasma between 300 nm and 900 nm was measured as a function of nitrogen flow into the plasma cell. The flow was varied from 1.0 to 10.0 sccm in 0.5 sccm increments. These spectra were evaluated to determine the relative proportions of nitrogen in an excited electronic state (N_2^*), nitrogen ions (N_2^+ and N^+), and electronically excited neutral atomic nitrogen (N°) as a function of nitrogen flow into the plasma cell. These results were compared to results obtained when the rf

source was first installed with the manufacturer's supplied orifice with 37 hole 0.5 mm in diameter and having a lower conductance than that used in the present study. The low conductance geometry has been used in studies of rf plasma grown GaN in other laboratories. [19,20]

The grown films were subject to structural, electrical, and optical characterization. KMAP x-ray studies provide information on crystal phase purity, stacking fault density and planar asymmetry. TEM studies provided more detailed information on the same properties for a few select samples as well as information on the structure of the interface. Atomic force microscopy (AFM) was used to evaluate the surface roughness and morphology. The rms roughness was measured over 1 and 5 μm squares. The results were typically independent of scan area to within 0.1 nm. Ellipsometry at the red HeNe 633 nm wavelength was used to measure the radial variation of film thickness and refractive index. The index appears to correlate strongly with GaN/GaAs interface quality. Most samples were fabricated into MIS capacitor structures and IV and CV measurements were made to assess the electrical properties of the GaN/GaAs interface.

Characterization of the RF Plasma Cell

The plasma source was characterized by measuring the optical emission from the plasma cell under various operating conditions. Emission spectra were measured between 300 and 900 nm. Of the many possible transitions for molecular and atomic nitrogen species only seven initial state configurations were observed. Not all species are detectable as they may have very long lifetimes or do not emit in the observable range. For a fixed power level of 300 W optical emission spectra from the plasma cell were recorded for flows from 1.0 to 10.0 sccm every 0.5 sccm. In all spectra emission associated with N_2^*, N_2^+, N°, and N^+ can be identified [21-23]. N_2^* is considered to be a significant species because initial state configuration of the 2nd positive system of N_2^* has an energy greater than that required to dissociate the bond. It has been speculated that N_2^* may play an active role in the growth of some nitrides. [24] Emission from the pure N_2 plasma in the 300-500 nm range is dominated by emission from the 2nd positive system of N_2^*. Many of these peaks overlap with emission lines from N_2^+, N°, and N^+. In the range 560-800 nm emission is dominated by the 1st positive series of N_2^*. Significant exceptions are the infrared afterglow (IRA, also referred to as the Y band) emission line at 674 nm and the N° emission line at 745 nm. The two significant features above 800 nm are emission from N°.

To allow a comparison of relative emission intensities an attempt was made to find characteristic emission lines for each specie which did not overlap with lines due to other nitrogen species. This was not always possible

and compromises had to be made. A representative emission spectrum is shown in Figure 1 for a nitrogen flow of 4 sccm. The purest representative lines are those for the 2nd positive system at 314 nm, the 1st positive system at 632 nm, the IRA line at 674 nm and the N° line at 825 nm. The lines chosen for N_2^+ (391 nm) and N^+ (464 nm) both contain some background from the 2nd positive system of N_2^*. The strongest line in the spectrum just below 360 nm mixes substantial contributions from N_2^* and N_2^+ while what appears to be the strongest N° line at 745 nm contains a strong N_2^* contribution. Some of the emission lines appearing in the present spectra are not found in the published spectra for similar plasma sources. This is attributed to differences in orifice plate geometry and plasma cell size as discussed below.

For an input power of 300 W the absolute intensities of the chosen lines of four species most likely to contribute to growth are shown in Figure 2. Each specie shows a unique functional dependence on flow rate. All increase sublinearly with flow and the ionic species saturate with increasing flow more rapidly than the neutral species. To consider the change in the relative intensities of emission lines a background intensity of 43.5 was subtracted from each spectrum. The 2nd positive system N_2^* line at 314 nm was chosen as a reference. This choice has two advantages. First, the concentration of N_2^* emitting in the 2nd positive system has been reported to correlate with the concentration of N° in the plasma. [25] Second, the strongest ionic emission lines both sit on a background due to 2nd positive system emission. As will be seen below, in contrast with neutral species, relative concentrations of ionic

species decrease with increasing gas flow. When the intensity of the ionic emission line no longer changes with increasing gas flow it is possible that the ionic emission has essentially dropped to zero and we are measuring only the N_2^* background.

The variation of the N_2^* 1st positive system, N_2^+, N^+ and N° with respect to the N_2^* 2nd positive system as a function of gas flow rate is shown in Figure 3. The variation of the intensity of the IRA line tracks that of the 1st positive system fairly closely and is not shown. From the figure it may be seen that the relative intensity of emission from the N_2^* 1st positive system increases slightly with increasing flow rate (as does the IRA emission) while the relative intensities of N_2^+ and N^+ decrease. Saturation of the N_2^+ signal occurs at about 8 sccm while saturation of the N^+ signal occurs at about 5.0 sccm.

Finally, we consider the relative performance of the plasma source with the low conductance orifice plate (LCOP) (37 x 0.5 mm holes). The LCOP data is included to facilitate comparison with growth studies performed by other groups using OAR sources. All growth experiments and the plasma data reported above pertain to the high conductance orifice plate (37 x 1 mm holes). For a given gas flow it took more power to light a plasma using the LCOP. Figure 4 illustrates a comparison at 300 W input power for a nitrogen flow rate of 2.0 sccm. Optical emission spectra were normalized to the N_2^* 2nd positive emission line at 314.1 nm. The most dramatic difference is the increase in the atomic nitrogen lines at 745 nm, 825 nm, and 868 nm using

the LCOP. Increases in the production of N_2^- and N^- are much smaller. The recorded absolute intensity of the emission from the LCOP was about two orders of magnitude brighter than for the high conductance orifice plate (HCOP) but this comparison must be qualified. Between the two measurements the tubulation providing the line-of-sight path from the plasma cell to the spectrometer was bent. Because the spectrometer could no longer be sighted along the axis of the plasma the difference in intensities is very likely exaggerated.

GaN/GaAs Interfaces

In the first series of experiments with plasma activated nitrogen both the Ga flux and the N_2 flow into the rf source were varied. Previous results with ammonia based growth implied that atomic nitrogen aggressively attacks GaAs. If this is true then higher nitride growth rates which bury the GaAs faster might result in better interfaces. Hence, the object was to look for stoichiometry related variations in crystal quality and growth rate related variations in interfacial smoothness and substrate damage[26,27] . In these experiments stoichiometry has to be interpreted broadly. Varying the nitrogen flow varies the relative concentrations of four chemically active nitrogen species. Each of these might be expected to have very different kinetic behaviors in the nucleation and growth of GaN.

A summary of the results is shown in Figure 5. The abscissa is the N_2 flow into the plasma cell and the ordinate is R_{N2}(GaN). Figure 5 plots nineteen experimental data points each labeled by a run number. The solid lines define a band in which pure βGaN nitride films were obtained. Below the band, degradation of the interface is observed. Above the band, columns of αGaN are observed embedded in the predominantly βGaN film. The dashed line denotes a boundary where the surface roughness abruptly increases and the refractive index decreases slightly. The variation of the dashed line is extrapolated by assuming it to be roughly parallel to the solid line boundaries. Identification of the phase boundary separating pure cubic and mixed cubic/hexagonal films is based on KMAP and TEM analysis.

Cross-sectional TEM images were made parallel and perpendicular to the major flat of the substrate. The substrates were SEMI specification with the major flat perpendicular to the $[1\bar{1}0]$ direction. All samples were found to contain high densities of stacking faults (SFs) on {111} planes. The SF density in cross-sections parallel to the major flat is typically an order of magnitude lower than the density observed in cross-sections perpendicular to the major flat. The asymmetry in stacking fault distribution could be due several factors: differences in the structure of α and β dislocations, their respective partials, or their mobilities.

Of the samples characterized by TEM, 356 and 359 had the most nearly perfect cubic crystalline structures. The TEM for 356 is shown in Figure 6. The stacking fault density decreases away from the substrate toward the top surface in a 20 nm thick interfacial layer. This suggests that the quality of the GaN layer increases with thickness for stoichiometric growth conditions. Arsenic doping of the interfacial GaN region may also decrease the stacking fault energy making formation of stacking faults more likely near the interface. The interface was rough on the scale of five monolayers laterally and vertically in the cross-section perpendicular to the major flat and substantially smoother in the orthogonal cross-section There did not appear to be any alloying between the GaAs and the GaN in any of the samples. Sample 383 was similar to 356 in both refractive index and surface roughness. The film quality is not too different than that of 356 but the interface is slightly rougher in both cross-sections. TEM images of sample 359 showed a

thinner film with the smoothest interface and the lowest stacking fault densities in both ⟨110⟩ directions of any sample in the study.

The results from the KMAP x-ray analysis are consistent with the TEM results. Figure 7(a) shows the KMAP for 356 with the x-ray line source parallel to the major flat. The strongest diffraction feature is the (002) reflection of cubic GaN. The distortion of the spot into a crescent shape is due to the high density of SFs in the crystal. For this orientation of the substrate the x-ray path intersects the higher density of SFs as they are diffracted. A similar distortion is observed by electron diffraction in the TEM. When sample 356 is rotated 90° the diffraction feature appears as shown in Figure 7(b). In this orientation the path of the x-rays intersects the low density of SFs and the feature is more nearly elliptical. The interesting distortion is directly below the center of the feature and is again due to the higher density of SFs which are now orthogonal to the x-ray path. The same is true for the TEM electron diffraction pattern for this orientation. KMAPs for other pure cubic samples are qualitatively the same with slightly broader diffraction features. The βGaN films are also well oriented with respect to the substrate. This is demonstrated by our ability to find asymmetric (113) reflections. In αAlN films grown with either ammonia or plasma N_2 we have never observed asymmetric reflections due to rotational disorder in the alignment of the 00.1) hexagonal basal plane with respect to the (001) cubic substrate surface.

A comparison of the samples grown with a nitrogen flow of 2.0 sccm illustrates the effect of varying the gallium flux for a fixed nitrogen flow into the plasma cell. TEM for these samples are taken in the cross-section perpendicular to the major flat which more clearly illustrate the defective structure. While the interface roughness is limited to a few monolayers, the GaAs substrate contains voids or pits which were probably formed due to the outdiffusion of Ga atoms into the GaN. The GaN layer also contains misoriented grains and a high density of stacking faults. Stacking faults originate at the interface and at grain boundaries. Twinned cubic and hexagonal grains were also observed near the interface while the top of the GaN layer was cubic. For the lowest Ga flux, 346, pyramidal pits are apparent in the GaAs substrate as seen in Figure 8(a). Small grains of hexagonal GaN are observed just above the interface. In sample 343, shown in Figure 8(b) with a higher Ga flux the pits appear to be semicircular and the interfacial hexagonal grains have disappeared. The films grown at the two highest fluxes, 356 and 357, are free of pits in the GaAs. TEM observations do not preclude the possibility of point defect damage in the GaAs.

Previously, in the work with ammonia at higher growth temperatures, such pits were associated with the extensive loss of Ga from the GaAs. Residual As was found to crystallize in the voids produced by the decomposition of the GaAs. Degradation of the GaAs under conditions of nitrogen rich nucleation and growth may cause the apparent increase in the measured film refractive index which assumes a perfect substrate and

interface. Pitting has been observed in other work with rf plasma sources but has not been reported for nitrides grown with ECR type sources [28,29]. Since ECR sources produce primarily N_2^+ ions it is suggested that pitting is a consequence of the attack of atomic nitrogen during nucleation and early stages of growth when the nitride film is thin enough to allow the indiffusion of atomic nitrogen.

Sample 357 was grown at the highest Ga flux for a nitrogen flow of 2.0 sccm and is shown in Figure 9. This layer shows no pits but does have relatively large grains of hexagonal GaN embedded in the predominately cubic film. The grains are columnar and appear roughly conical near their origin. The apex is typically seen at or near the GaAs/GaN interface. Thus, the layer has a columnar structure with the lateral size of the grains equal to 15-20 nm. Ga-rich nucleation promoted twice as rough an interface in comparison with stoichiometric growth because of the high affinity of N to Ga. It also leads to multiple twinning and formation of areas of the hexagonal phase during the initial stage of GaN growth. Hexagonal grains (Figure 9) often tower over the (001) βGaN surface by 3-7 nm resulting in a rough surface morphology. The axis of the column corresponds to the (00.1) direction of the αGaN crystal and is parallel to the (001) growth axis of the βGaN film. This result is consistent with previous reports that Ga rich growth results in mixed phase films.

The KMAP peaks for samples 346, 343, 356, and 357 are shown in Figure 10. The samples were oriented so that the diffraction senses the stacking faults densities illustrated in the TEM images above. The crescent shape distortion diagnostic of a high stacking fault density is apparent for each sample. Samples 346 and 357 both have a second feature below the cubic (002) spot corresponding to the hexagonal phase (00.2) diffraction feature. This feature is stronger for sample 357 which is consistent with the higher fraction of hexagonal GaN observed by TEM.

The KMAPs for 360 and 382 are qualitatively similar to the KMAP for 357. Samples 357 and 382 have similar intensity in the (002) peak while the intensity of 360 is 5-10% weaker. This correlates with the ellipsometric result that 360 is about 10% thinner than the other two. Samples 373 and 374 both have (00.2) peaks appearing in their KMAPs, however, the more intense (002) peaks are more nearly elliptical than in all other samples. This suggests that the formation of extended planar defects, i.e. stacking faults, has been suppressed in favor of smaller crystalline domains. Finally, samples 346 and 390, grown under relatively nitrogen rich conditions also have hexagonal inclusions. The intensity and shape of the (002) peak of 346 clearly suggests the presence of stacking faults. The (002) intensity of 390 is the weakest of any other sample measured from this set. The appearance of the hexagonal phase in 346 and 390 is attributed to the rapid degradation of the GaAs substrate under extremely nitrogen rich nucleation conditions. Some correlation with the appearance of "pits" in the substrate as observed in 343 and 346 by TEM is

expected. The greater degradation of 390 as compared to 346 supports the hypothesis that substrate degradation is associated with atomic nitrogen.

The radial thickness variation of the epitaxial films has been measured by ellipsometry. Results for eight of the crystals near the boundary separating the pure cubic from the mixed phase nucleation are shown in Figure 11. Pure cubic phase crystals are shown with solid lines while mixed phase crystals are represented with dashed lines. Most of the crystals decrease monotonically in thickness moving outward from 0.1 in to 0.9 in. from the center of the substrate. Some crystals show a slight decrease in film thickness exactly at the center of the wafer. The radial decrease in film thickness is typically 15-20%, center-to-edge. The smoother films with the lowest refractive index appear to be the most nonuniform. In all cases but one the thickness appears to decrease monotonically. Sample 383 deviates from this functional form being too thick at large radii. All of the samples nucleated and grown with a high nitrogen to gallium flux ratio show similar behavior. All mixed phase samples grown with a low nitrogen to gallium flux ratio and not shown in Figure 11 show only the monotonic behavior.

The radial variation of the refractive index of the same set of samples was also characterized. The better samples typically have lower refractive indices and unlike the thickness variation the better samples show less variation center-to-edge. Some of the radial variation may be due to the interpretation of the measurement which assumes uniform planar films of GaAs and GaN with perfect interfaces and smooth surfaces. In the mixed

phase films some of the variation in the index may also reflect a variation in the fraction of the hexagonal phase which has an index slightly lower than that of the cubic phase. The correlation between rms surface roughness and the wafer center refractive index for is shown in Figure 12. The solid circles represent films grown with nitrogen flow rates in the range of 2-5 sccm. The normal (pointing up) triangles represent films grown at a flow rate of 1 sccm where the plasma contains the highest proportion of ionic species (347, 355). The inverted triangles (pointing down) represent films grown at 7.5 sccm where the plasma is saturated with neutral species (382, 383, 389, 390). Films grown with 2-5 sccm nitrogen flows follow a square root dependence of rms roughness, R, on index measured at 633 nm. The best know value for βGaN at this wavelength is 2.385 as determined by Köhler et al.[30] The fit minimizes at n = 2.368 with the lowest measured value being n = 2.378 for sample 359. All other values are greater than 2.385.

The extreme outlier is 390 which is the only sample in Figure 12 grown in the nitrogen rich regime with interfacial αGaN grains. The indexes of the other samples falling in this region, 346 and 348 (see Figure 5), could not be evaluated by the ellipsometer using a two layer model. These samples had rms roughnesses of 43 and 25 Å, respectively. The samples grown in the 2-5 sccm region with the square root variation of roughness with index are primarily single phase βGaN with smooth GaN/GaAs interfaces. Samples grown under nitrogen rich conditions with interfacial αGaN grains have the

roughest surfaces with high or unmeasurable interfaces. Films nucleated under ion rich conditions are worse than films nucleated under neutral rich conditions. The index of 348 cannot be measured, that of 390 can although the surface is rougher. The four 37x samples grown at 7.5 sccm which are not shown in Figure 12 are rough, 22-40 Å rms, have measurable indices of about 2.4 which do not correlate with the roughness. Sample 347 in the pure βGaN region of the map is rougher than any similar sample grown in the 2-5 sccm range and 355 is rougher than 357 or 360.

With the exception of sample number 379, MIS capacitors were fabricated from all of the films and their I-V and C-V characteristics were measured. Concerning I-V characteristics the following observations are made. All samples are leaky. The best samples exhibit much higher leakage. The current behavior has the form of Schottky emission with an apparent activation energy of 0.7 eV for the best samples and about 0.8 eV for the other samples. This is consistent with the estimation that the conduction band offset is about +0.2 eV going from GaAs to GaN[31]. From the C-V characteristics it is found that none of the samples show significant modulation of the Fermi level at the GaN/GaAs interface. The poorer samples behave as if the Fermi level is pinned in the upper half of the GaAs band gap. Nitridization of GaAs with and ECR plasma source has been shown to introduce several traps in the upper half of the GaAs band gap[32]. The best samples (assuming the ellipsometric thicknesses are accurate) behave as though the Fermi level is pinned near the GaAs conduction band

and that there is a high density of defect states in the GaN. The high capacitance measured for these samples would require incomplete depletion in the GaN layer. This would occur if the defect state density in the GaN were at a level of at least $1x10^{18}/cm^3$ which is not unreasonable.

With reference to Figure 5 the best samples are 347, 356, 358, 359, 383, and 389. Better samples are closer to the boundary separating the pure βGaN films and the mixed phase films grown under Ga rich conditions. I-V data for films grown at 4.0 sccm, or more, and close to the pure/mixed boundary are shown in Figure 13. Pure cubic films are shown as solid lines and mixed phase films as dashed lines. The pure cubic films tend to have more nearly ideal Schottky characteristics than mixed phase films and mixed phase films grown at nitrogen flows greater than 4.0 sccm are significantly better than those grown below 4.0 sccm. The latter fact is attributed to neutral rich growth above 4.0 sccm. The best characteristic associated with sample 359 is additionally marked by diamonds. This sample had the most nearly ideal C-V characteristic and was the only sample in which the nitride thickness extracted from the capacitance measurement was in close agreement with the thickness determined by ellipsometry.

Overall, the combined results suggest that the best nucleation and growth occurs for conditions close to that used for sample 359. This sample is pure cubic GaN very close to the cubic/Ga rich mixed phase boundary. The active nitrogen flux is just about to saturate with increasing N_2 flow. The surface is smooth and the refractive index is the smallest with the least

variation across the substrate of any sample. The electrical characteristics are consistent with Schottky transport over a small n-type GaN barrier separating the GaAs and the metal. Samples grown at higher nitrogen flows seem to be better than those grown at lower flow rates suggesting that relative concentrations of ionic and neutral nitrogen species is important.

Discussion of Plasma Activated Nucleation and Growth

The goal of the activity was to achieve an abrupt electrically neutral interface between GaAs and GaN. The first step is the formation of an atomically abrupt and smooth interface. With the exception of monolayer islands of GaN embedded in a GaAs matrix there are few demonstrations of abrupt planar interfaces between GaAs and GaN.[12,13,33-35] The only comparable results are for an ultrathin (5-7 monolayers) GaN film also grown by plasma assisted MBE.[36] The TEM cross-section of sample 356 parallel to the major flat has the smoothest interface and possibly the lowest stacking fault density ever demonstrated for GaN layers of comparable or greater thickness grown on GaAs. This comparison includes all reports of GaN on GaAs including samples grown by MOCVD, plasma assisted MOCVD and MOMBE, and plasma assisted GSMBE.

Another criterion these nitride films should satisfy is that they be of uniform thickness and have smooth surfaces. Sample 359 has an rms surface roughness of only 4 Å. Despite this fact the RHEED patterns along the two orthogonal (110) directions were not identical. They were not as streaky as others demonstrated in the literature for GaN on GaAs and at no time was a reconstruction other than (1 × 1) ever observed during growth of GaN. Streaky (2 × 2) reconstructions for growth on GaAs substrates have been reported for growth from a dc glow discharge or ECR plasma source [11,37]. The (2 × 2) reconstruction is associated with an As/N stabilized surface while a c(2

× 2) reconstruction may be associated with an As induced Ga stabilized surface.[38] TEM shows very rough interfaces between the substrates and the overlayers. Using an ECR source smooth surfaces have been shown to be due to bombardment of the epitaxial surface by energetic nitrogen ions. By tuning the ion energy the crystallinity and planarity of the GaN may be optimized.[39]

Relative to ECR sources the rf source used in the present study produces a much higher concentration of neutral species and presumably all species have a lower kinetic energy component as they reach the substrate. This is a consequence of eliminating the magnetic fields accelerating ions in the direction of the substrate. In this respect rf sources may be superior to other types of plasma sources as it has also been shown that while ion bombardment of the film promotes smooth surfaces it also introduces lattice damage in the nitride films which does not anneal out at temperatures low enough to be compatible with growth on GaAs substrates.

The issue of planarity appears to be a serious one for the rf plasma source. The best films are also the most nonuniform in thickness. Similar nonuniformity has been reported by Foxon and coworkers using the same type of plasma cell with a LCOP. Their results were determined by optical reflectance measurements assuming a refractive index of 2.3 for the GaN [20,40]. This effect may be primarily due to the use of high pressure (plasma) gas injector as reported by Panish and Sumski for the growth of GaInAsP using thermally cracked arsine and phosphine [41]. The degree of As_2/P_2 flux nonuniformity was sensitive to the geometry of the effusion end of their gas

injectors and fell off much faster than a cosine distribution. Foxon's group has noted that the nonuniformity is greater for higher nitrogen flows while a dependence on both nitrogen and gallium fluxes has been observed in the present work.

The nonuniformity doesn't seem to be related to scattering of the Ga beam by the nitrogen as the nonuniformity is insensitive to increases in the nitrogen flux which strongly affect the amount of Ga scattered away from the substrate. Al is more strongly scattered than Ga is and the nonuniformity of AlN films is typically 25-30% as compared to 15-20% for GaN films. Another possibility is that the growth rate is dependent on the profile of a particular nitrogen specie. Certainly, the neutral species N_2^* and N° will be concentrated along the axis of the beam path while N_2^+ and N^+ will have increasingly broad profiles due to simple electrostatic repulsion between the ions as they move toward the substrate. Some of the nonmonotonic thickness variations may ultimately be found to correlate with the different profiles of the various active nitrogen species.

The nucleation and growth experiments produced several interesting results which were not anticipated from past experience with other III-V heteroepitaxial system. The first is the dramatic dependence of thickness and uniformity as a function of Ga flux for a fixed nitrogen flow into the plasma cell. The second is that as the growth conditions become increasingly Ga rich the interface quality, as measured by the refractive index, first deteriorates and then apparently improves. Finally, for a fixed substrate temperature and

input plasma power there is a well defined point in the Ga flux/N_2 flow phase space at which the nucleation and growth is optimized. The best explanation assumes that these results are all a consequence of there being several different reactive nitrogen species in the plasma stream which interact differently with the substrate and with metallic Ga supplied during film growth.

The best sample, number 359, lies close to the boundary separating the nucleation of pure cubic GaN from the nucleation of mixed phase films. It has lowest index, the smoothest surface and the smallest optical thickness of any sample (374 may be slightly thinner). The best film grown at a higher nitrogen flow, 383, was grown at almost exactly the same Ga flux. In all respects it is only slightly worse than 359. This is consistent with the saturation of active nitrogen with increasing flow as illustrated in Figure 14. The experimental points corresponding to pure cubic epitaxy are represented as open squares and the mixed phase films as solid triangles. From Figure 5 it is evident that there is a ridge in the growth rate vs. N_2 flow response surface on which the crystallinity of the cubic phase and the planarity of the interface is superior. Electrical characterization of the films on the ridge indicate that of these films those grown at or near an N_2 flow of 4.0 sccm are the best and flows greater than 4.0 sccm are better than lower flows. To look for a correlation with the variation of individual nitrogen species in the plasma stream the relative variations of N°, N_2^* and N_2^+ were all normalized to pass through the point (0.44, 4.0) on the R_{N2} vs. N_2 flow diagram. N° is plotted as a

dashed line, N_2^* as a chain line, and N_2^- as a solid line. The N_2^+ variation easily separates the pure cubic samples from the mixed phase films nucleated under Ga rich conditions. From this it is inferred that N_2^+ is the single most important nitrogen specie in the present experiment. Assuming that N° is more important than N_2^* in then it may be assumed that optimal films are obtained for a particular N°/N_2^+ ratio.

Sample 359 was the thinnest nitride film in the study. It had the largest center-to-edge thickness nonuniformity associated with one of the most uniform center to edge index variations. The RHEED diffraction was very streaky as compared to other samples. It had the smoothest surface as measured by AFM. Of all the samples with Schottky like I-V characteristics it had the lowest reverse leakage current. The C-V response for 359 was the most nearly ideal with the measured insulator capacitance most closely corresponding to that estimated from the optical thickness. Figure 14 shows that the N_2^- variation can be used to define a boundary between the pure cubic and mixed phase crystals. At higher nitrogen flows the N_2^* variation comes very close to exactly separating those mixed crystals for which the index and roughness correlate (below the line) for those mixed crystals for the index and roughness anticorrelate (above the line).

It has been previously noted that the electrical behavior of films grown at flows greater than 4.0 sccm are qualitatively different from those grown at flows below 4.0 sccm. This is most immediately obvious when comparing the radial thickness of 383 with all of the "good" samples grown at low flows.

The I-V characteristics of the best mixed phase samples grown at low flows were much worse than those of the best mixed phase samples grown at high flow. Finally, the C-V response of both the cubic and mixed phase films were superior when the films were grown at higher flows as compared to lower flows. Figure 14 was drawn with the intent demonstrating the role of different nitrogen species in determining the phase purity of the nitride films. All of the qualitative differences described above suggest that a transition from ion rich flow to a neutral rich flow does indeed occur.

This is further emphasized in Figure 12 where the rms surface roughness is plotted as a function of index. Note that while there is an excellent correlation for films grown at flows between 2.0 and 5.0 sccm the films grown at 1.0 sccm are much rougher than expected. Films grown at 7.5 sccm are slightly rougher than expected except for sample 390. These results can be explained in terms of the effect of energetic ions smoothing the surface during growth. Molnar and Moustakas have studied the morphology of GaN grown with an ECR source as a function of ion energy. ECR sources produce more N_2^+ than any other active nitrogen specie with the possible exception of N_2^*. At low ion energies the surface was rough from island growth. As the ion energy was increased the surface became smooth and at the highest energies the surface roughened again. In this study we find that concentrations of both N_2^+ and N^+ at 1.0 sccm are double the concentrations observed at 2.0 sccm as seen in Figure 3. This suggests that ion damage is significant at 1.0 sccm, that ion assisted planarization of the surface is

optimized at 4.0 sccm and that at 7.5 sccm it has decreased to the point where islanding is beginning to affect the morphology.

Conclusions

The synthesis of an unfaulted GaN film on a GaAs substrate is extremely difficult. A survey of the extant literature on the nucleation and growth of nitrides on GaAs has not revealed a single chemically active nitrogen source which does not appear to attack the substrate while simultaneously producing crystalline nitride overgrowth. The problem is minimized for the growth of GaN on GaAs. For this pair there is no chemical gradient in the cation profile and GaN is the most covalent of the nitrides. This minimizes the interface dipole resulting from the large difference in the electronegativity between As and N. An interfacial dipole may be the actual driving force for interface degradation.[42]

The results presented here have been discussed in terms of stoichiometric, Ga-rich, and As-rich growth. These terms are not technically correct as they follow from the assumption that the best crystals will be nucleated under a 1:1 Ga:N flux ratio. Using a plasma nitrogen source stoichiometry is a poorly defined concept given the presence of several active nitrogen species. Also, only unreconstructed (1×1) GaN surfaces were observed during film growth. It has been shown that growth with $c(2 \times 2)$ reconstructed surfaces (Ga rich surfaces) are associated with better optical properties. This implies that nucleation and growth must be optimized separately.

The essential conclusions drawn from the present study are that a) the relative concentrations of the nitrogen plasma species is an important

parameter in characterizing the growth kinetics of cubic GaN; b) nucleation under excessively nitrogen rich conditions causes degradation of the GaAs substrate while nucleation under excessively gallium rich conditions causes the growth of mixed phase films; c) the use of As to promote the formation of the cubic phase is necessary only during the first few monolayers for growth at 620 °C; and d) single wavelength ellipsometry provides a fast, sensitive, and nondestructive measure of thin film/interface quality.

Acknowledgements

Sandia is a multiprogram laboratory operated by Sandia Corporation a Lockheed Martin Company, for the United States Department of Energy under Contract DE-AC04-94AL85000. The authors would like to thank J. Mirecki-Millunchick for assistance in the nucleation and growth experiments. A. J. Howard performed the atomic force microscopy for the characterization of the surface roughness.

References

[1] B. W. Dodson, D. R. Myers, A. K. Datye, V. S. Kaushik, D. L. Kendall, and B. Martinez-Tovar, Phys. Rev. Lett. **61**, 2681 (1988).

[2] J. M. Moison, C. Guille, M. Van Rompay, F. Barthe, F. Houzay, and M. Bensoussan, Phys. Rev. B **39**, 1772 (1989).

[3] M. Yano, H. Yokose, Y. Iwai, and M. Inoue, J. Crystal Growth **111**, 609 (1991).

[4] A. Mazuelas, L. Gonzálèz, F. A. Ponce, L. Tapfer, and F. Briones, J. Crystal Growth **131**, 465 (1993).

[5] C. H. Yan, A. Y. Lew, E. T. Yu, and C. W. Tu, J. Crystal Growth **164**, 77 (1996).

[6] A. Bourret, and P. H. Fuoss, Appl. Phys. Lett. **61**, 1034 (1992).

[7] M. Aindow, T. T. Cheng, N. J. Mason, T.-Y. Seong, and P. J. Walker, J. Crystal Growth **133**, 168 (1993).

[8] J. M. Kang, M. Nouaoura, L. Lassabatère, and A. Rocher, J. Crystal Growth **143**, 115 (1994).

[9] C. J. Kiely, J.-L. Chyi, A. Rockett, and H. Morkoç, Phil. Mag. A **60**, 321 (1989).

[10] R. J. Hauenstein, D. A. Collins, X. P. Cai, M. L. O'Steen, and T. C. McGill, Appl. Phys. Lett. **66**, 2861 (1995).

[11] O. Brandt, H. Yang, B. Jenichen, Y. Suzuki, L. Däweritz, and K. H. Ploog, Phys. Rev. B **52**, R2253 (1995).

[12] Z. Z. Bandic, R. J. Hauenstein, M. L. O'Steen, and T. C. McGill, Appl. Phys. Lett. **68**, 1510 (1996).

[13] Z. Z. Bandic, T. C. McGill, R. J. Hauenstein, and M. L. O'Steen, J. Vac. Sci. Technol. B **14**, 2948 (1996).

[14] S. Gwo, H. Tokumoto, and S. Miwa, Appl. Phys. Lett. **71**, 362 (1997).

[15] Q.-K. Xue, Y. Hasegawa, I. S. T. Tsong, and T. Sakurai, Jpn. J. Appl. Phys. **36**, L1486 (1997).

[16] A. D. Bykhovski, and M. S. Shur, Appl. Phys. Lett. **69**, 2397 (1996).

[17] Y. Yamauchi, K. Uwai, and N. Kobayashi, Jpn. J. Appl. Phys. **35**, L80 (1996).

[18] T. S. Cheng, L. C. Jenkins, S. E. Hooper, C. T. Foxon, J. W. Orton, and D. E. Lacklison, Appl. Phys. Lett. **66**, 1509 (1995).

[19] H. Liu, A. C. Frenkel, J. G. Kim, and R. M. Park, J. Appl. Phys. **74**, 6124 (1993).

[20] S. E. Hooper, C. T. Foxon, T. S. Cheng, L. C. Jenkins, D. E. Lacklison, J. W. Orton, T. Bestwick, A. Kean, M. Dawson, and G. Duggan, J. Crystal Growth **155**, 157 (1995).

[21] A. N. Wright, and C. A. Winkler, Active Nitrogen (New York: Academic) 1968.

[22] R. W. B. Pearse, and A. G. Gaydon, The identification of molecular spectra (Fourth ed.) (London: Chapman and Hall) 1976.

[23] R. C. Weast (Ed.)., CRC Handbook of Chemistry and Physics, (Sixtieth ed.) (Boca Raton, Florida: CRC Press) 1980.

[24] W. C. Hughes, J. Rowland, W. H., M. A. L. Johnson, S. Fujita, J. Cook, J. W., J. F. Schetzina, J. Ren, and J. A. Edmond, J. Vac. Sci. Technol. B **13**, 1571 (1995).

[25] W. E. Hoke, P. J. Lemonias, and D. G. Weir, J. Crystal Growth **111**, 1024 (1991).

[26] S. Ruvimov, Z. Liliental-Weber, J. Washburn, T. J. Drummond, M. Hafich, and S. R. Lee, In F. A. Ponce, T. D. Moustakas, I. Akasaki, and B. A. Monemar (Eds.), III-V Nitrides, 449 (pp. 251). Boston, Massachusetts, U.S.A.: Materials Research Society (1997).

[27] S. Ruvimov, Z. Liliental-Weber, J. Washburn, T. J. Drummond, M. Hafich, and S. R. Lee, Appl. Phys. Lett. **71**, 2931 (1997).

[28] D. M. Tricker, P. D. Brown, T. S. Cheng, C. T. Foxon, and C. J. Humphreys, Appl. Surf. Sci. **123/124**, 22 (1998).

[29] L. C. Jenkins, T. S. Cheng, C. T. Foxon, S. E. Hooper, J. W. Orton, S. V. Novikov, and V. V. Tret'yakov, J. Vac. Sci. Technol. B **13**, 1585 (1995).

[30] U. Köhler, D. J. As, B. Schöttker, T. Frey, K. Lischka, J. Scheiner, S. Shokhovets, and R. Goldhahn, J. Appl. Phys. **85**, 404 (1999).

[31] S. A. Ding, S. R. Barman, K. Horn, H. Yang, B. Yang, O. Brandt, and K. Ploog, Appl. Phys. Lett. **70**, 2407 (1997).

[32] Y. J. Park, E. K. Kim, I. K. Han, S.-K. Min, P. O'Keeffe, H. Mutoh, H. Munekata, and H. Kukimoto, Appl. Surf. Sci. **117/118**, 551 (1997).

[33] M. Sato, Sol. St. Electron. **41**, 323 (1997).

[34] M. Sato, Jpn. J. Appl. Phys. **34**, 1080 (1995).

[35] T. Makimoto, and N. Kobayashi, Appl. Phys. Lett. **67**, 688 (1995).

[36] O. Brandt, H. Yang, A. Trampert, M. Wassermeier, and K. H. Ploog, Appl. Phys. Lett. 71, 473 (1997).

[37] S. Strite, J. Ruan, Z. Li, A. Salvador, H. Chen, D. J. Smith, W. J. Choyke, and H. Morkoç, J. Vac. Sci. Technol. B 9, 1924 (1991).

[38] G. Feuillet, H. Hamaguchi, K. Ohta, P. Hacke, H. Okumura, and S. Yoshida, Appl. Phys. Lett. 70, 1025 (1997).

[39] R. J. Molnar, and T. D. Moustakas, J. Appl. Phys. 76, 4587 (1994).

[40] D. E. Lacklison, J. W. Orton, I. Harrison, T. S. Cheng, L. C. Jenkins, C. T. Foxon, and S. E. Hooper, J. Appl. Phys. 78, 1838 (1995).

[41] M. B. Panish, and S. Sumski, J. Appl. Phys. 55, 3571 (1984).

[42] T. Maeda, H. Tanaka, M. Takikawa, and K. Kasai, J. Crystal Growth 150, 649 (1995).

Figure Captions

Figure 1) Optical emission spectra for the OAR plasma source using the high conductance orifice plate running 4 sccm of N2 at 300 W of rf power.

Figure 2) Absolute emission intensity from the OAR plasma source of the characteristic emission lines for atomic and molecular species as a function of nitrogen flow into the plasma cell at 300 W of rf power.

Figure 3) The characteristic emission lines for atomic and molecular species shown in Figure 5 normalized to the intensity of the N_2^* 2^{nd} positive emission.

Figure 4) Comparison of the spectra obtained from the OAR plasma source using the high conductance orifice plate used in this study (37x1.0 mm holes) with the low conductance orifice plate (37x0.5 mm holes) which is standard for this plasma source.

Figure 5) A response surface for the nucleation of βGaN on GaAs under an initial As flux. Each data point is labeled with a run number. The solid lines are the upper and lower bounds of the region in which pure cubic films were obtained. The dashed line marks a boundary above which substantial surface roughening occurs the variation at low flows simply assumes it to be parallel to the solid line boundaries.

Figure 6) Cross-sectional high resolution TEM images (top) and corresponding electron diffraction patterns (bottom) of sample 356 perpendicular (a, c) and parallel (b, d) to the SEMI spec major flat. The streaks at (111) diffraction spots in (c) are arising from stacking faults whose density is

typically higher for "perpendicular" cross-sections (a) as compared to the cross-section parallel to the major flat (b). Not streaks are visible in (d).

Figure 7) X-ray KMAPs of sample 356 with the x-ray line source parallel to (a) and perpendicular to (b) the SEMI spec major flat. The crescent shaped distortions in (a) and the distortion below the central peak in (b) are both a consequence of the high stacking fault density observed in Figure 6.

Figure 8) Cross-sectional high resolution TEM images of samples 346 (a) and 343 (b) perpendicular to the SEMI spec major flat. Sample 346 was nucleated nitrogen rich relative to 356 and shows some pitting of the GaAs substrate and hexagonal grains (αGaN) near the interface which are overgrown by cubic GaN. For sample 343 (b) the Ga to N flux ratio during nucleation was intermediate to 356 and 346. Pitting of the substrate is still observed, but the formation of hexagonal grains has been suppressed.

Figure 9) High resolution TEM image (a) and corresponding electron diffraction pattern (b) of sample 357 perpendicular to the SEMI spec major flat. This sample was nucleated gallium rich relative to 356 and shows large hexagonal grains nucleating at or near the interface which are not overgrown by cubic GaN. There is no evidence of pitting in the GaAs substrate.

Figure 10) X-ray KMAPs of samples 346 (a), 343 (b), 356 (c), and 357 (d) with the x-ray line source parallel to the SEMI spec major flat. Features due to the (00.2) reflection of hexagonal GaN are observed in the maps of 346 and 357.

Figure 11) Ellipsometric thickness variation as a function of radial distance from wafer center for several GaN films. Solid lines indicate pure cubic films while dashed lines indicate mixed phase films.

Figure 12) The rms surface roughness shows a square root dependence on wafer center refractive index for wafers grown with nitrogen fluxes in the range of 2-5 sccm.

Figure 13) Current density vs. applied bias for several Schottky/GaN/GaAs diodes. Solid lines indicate pure cubic films while dashed lines indicate mixed phase films.

Figure 14) The measured intensity variation of three plasma nitrogen species are plotted assuming equal concentrations at a nitrogen flow of 4.0 sccm where the best films were obtained. Point on the response surface representing pure cubic films are shown as open squares. Mixed phase films are shown as solid triangles. All cubic films fall below the N_2^+ boundary. At fluxes above 7.0 sccm the N_2^* boundary closely follows the smooth rough boundary drawn in Figure 5.

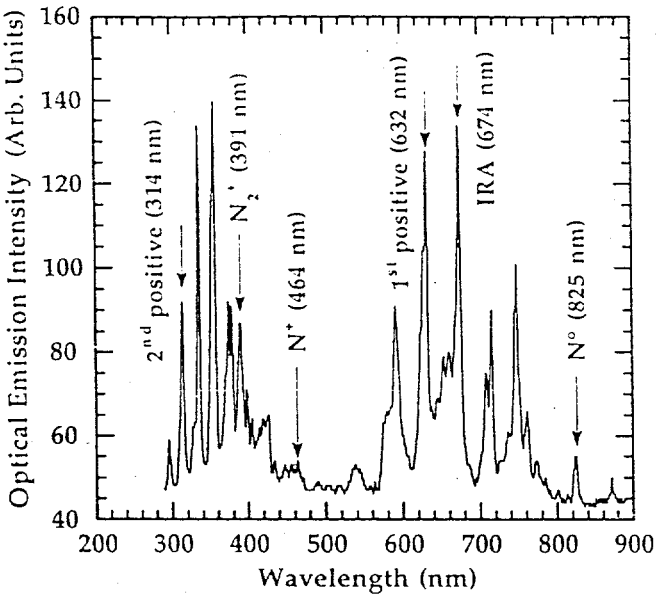
Optical Emission Intensity (Arb. Units)
160
140
120
100
80
60
40
200
300
400
500
600
700
800
900
Wavelength (nm)
2nd positive (314 nm)
N2' (391 nm)
N+ (464 nm)
1st positive (632 nm)
IRA (674 nm)
N° (825 nm)

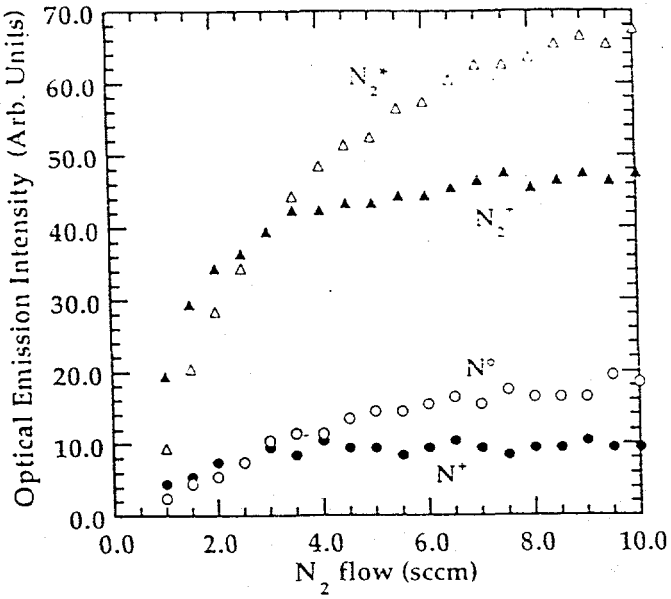
Optical Emission Intensity (Arb. Units)
70.0
60.0
50.0
40.0
30.0
20.0
10.0
0.0
0.0
2.0
4.0
6.0
8.0
10.0
N2 flow (sccm)
N2+
N2
N°
N+

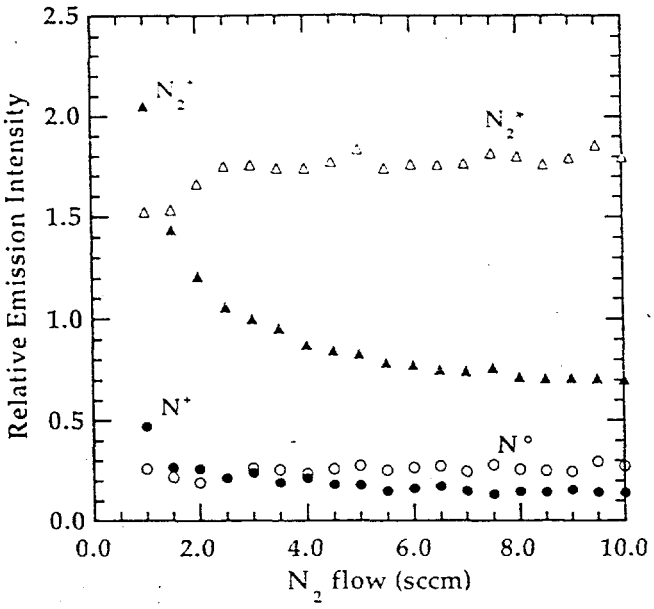
Relative Emission Intensity
2.5
2.0
1.5
1.0
0.5
0.0
N_2^+
N_2^*
N^+
N°
0.0
2.0
4.0
6.0
8.0
10.0
N_2 flow (sccm)

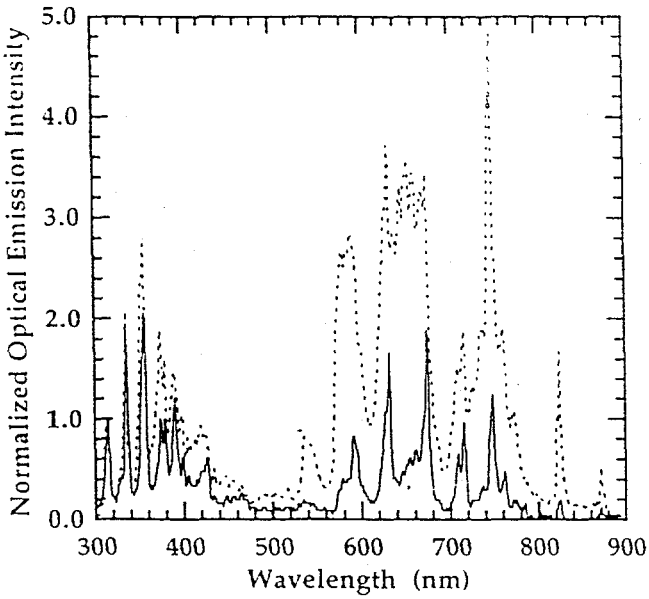
Normalized Optical Emission Intensity
5.0
4.0
3.0
2.0
1.0
0.0
300
400
500
600
700
800
900
Wavelength (nm)

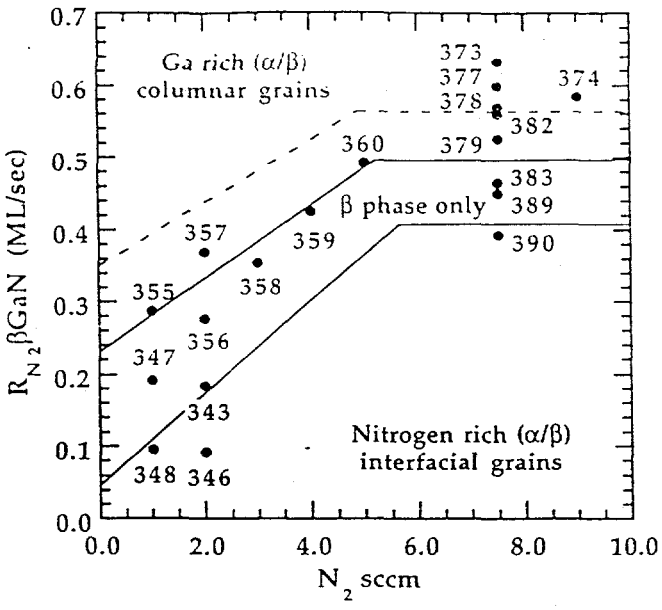
Ga rich (α/β)
columnar grains
β phase only
Nitrogen rich (α/β)
interfacial grains
R_{N_2}βGaN (ML/sec)
N_2 sccm
0.0
0.1
0.2
0.3
0.4
0.5
0.6
0.7
0.0
2.0
4.0
6.0
8.0
10.0
373
377
378
374
382
360
379
383
389
357
359
390
355
358
356
347
343
348
346

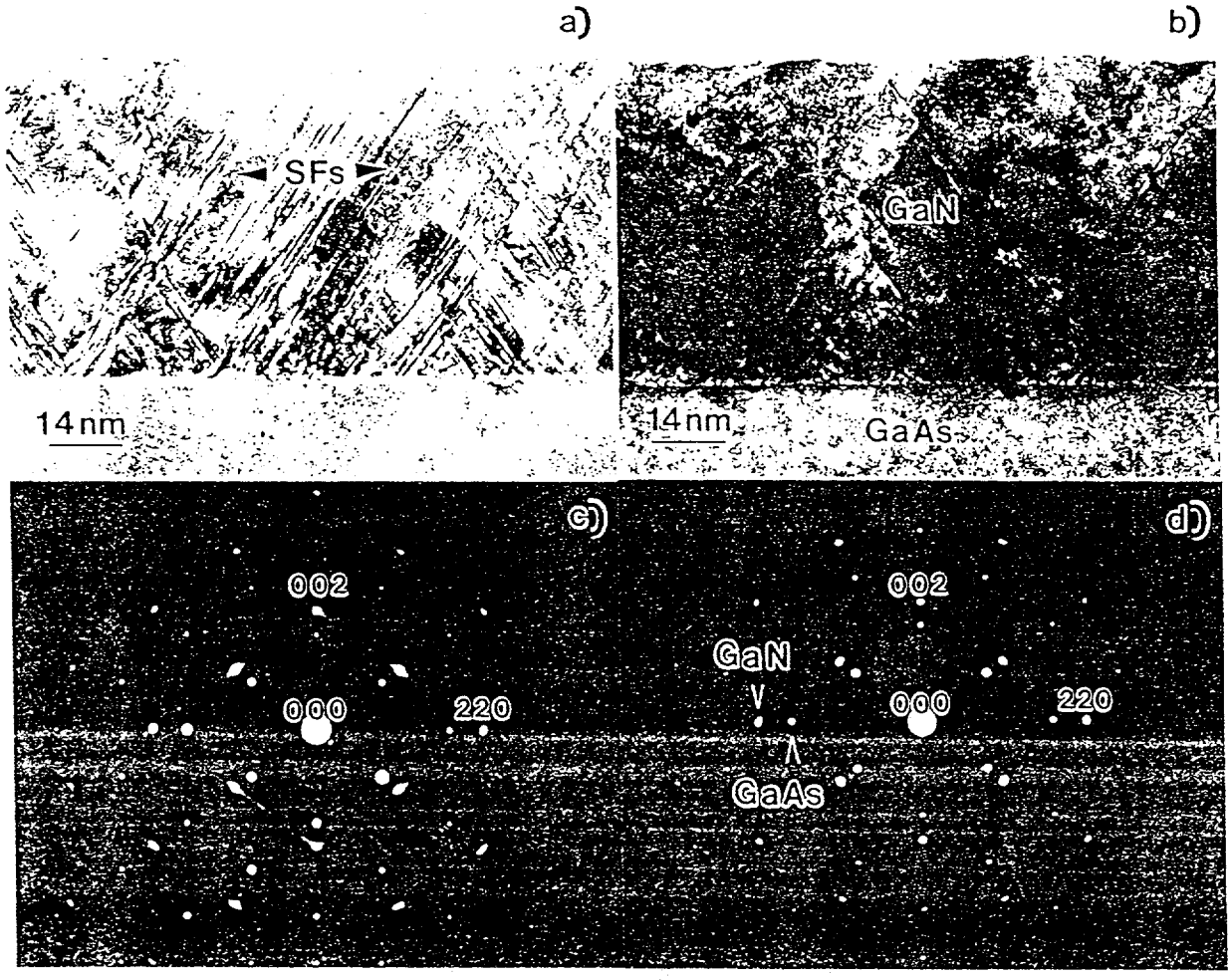
a)
b)
SFs
14nm
GaN
14nm
GaAs
c)
d)
002
000
220
GaN
GaAs
002
000
220

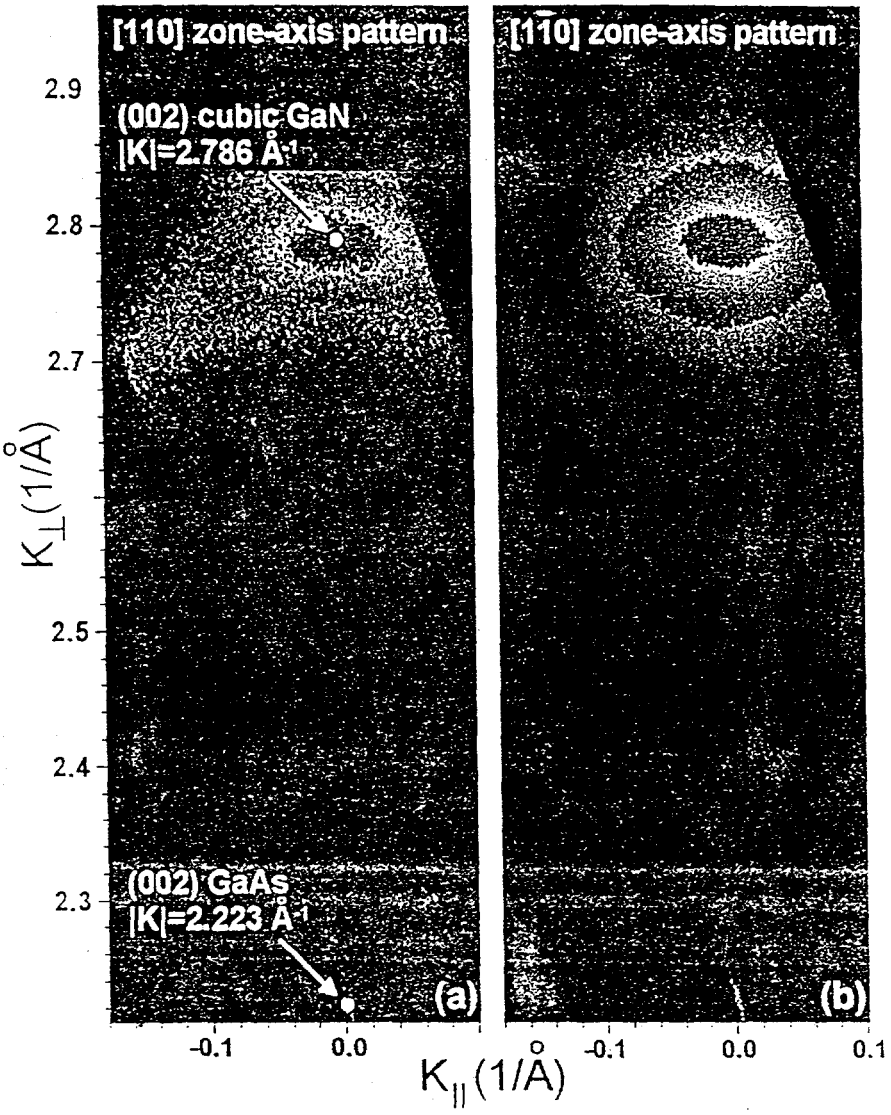
[110] zone-axis pattern
(002) cubic GaN
|K|=2.786 Å-1
(002) GaAs
|K|=2.223 Å-1
(a)
[1$\bar{1}$0] zone-axis pattern
(b)
2.9
2.8
2.7
2.5
2.4
2.3
K⊥(1/Å)
-0.1
0.0
-0.1
0.0
0.1
K|| (1/Å)

a)

b)

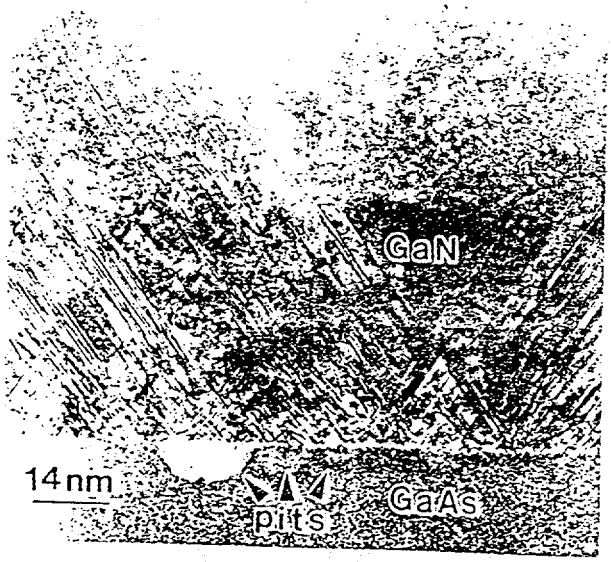

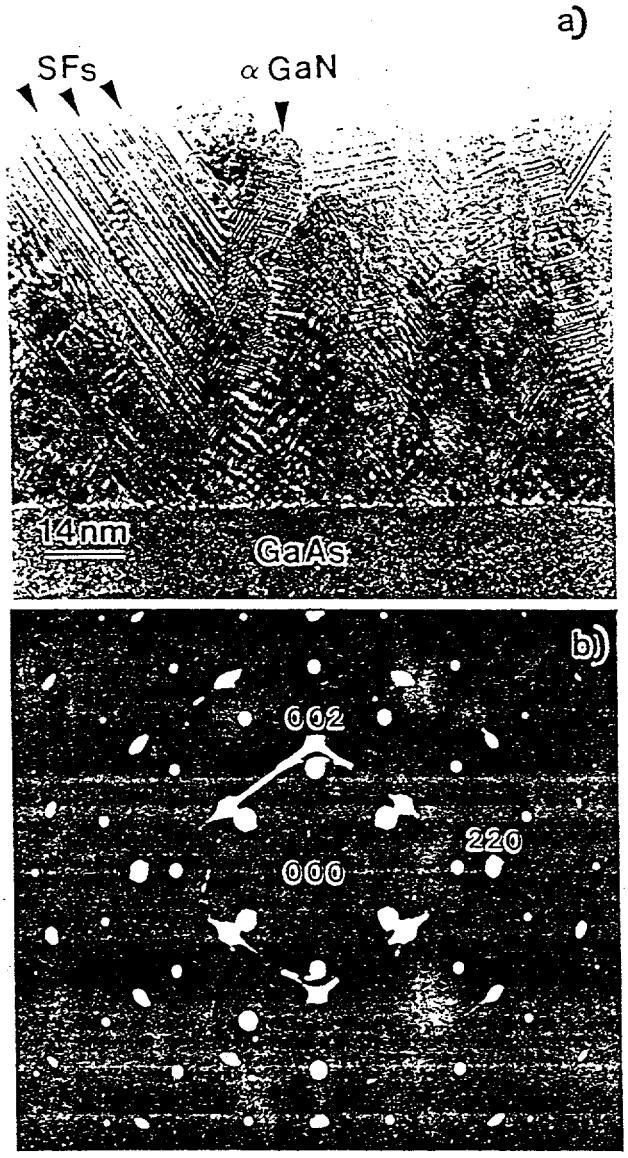
a)
SFs
α GaN
1.4nm
GaAs
b)
002
220
000

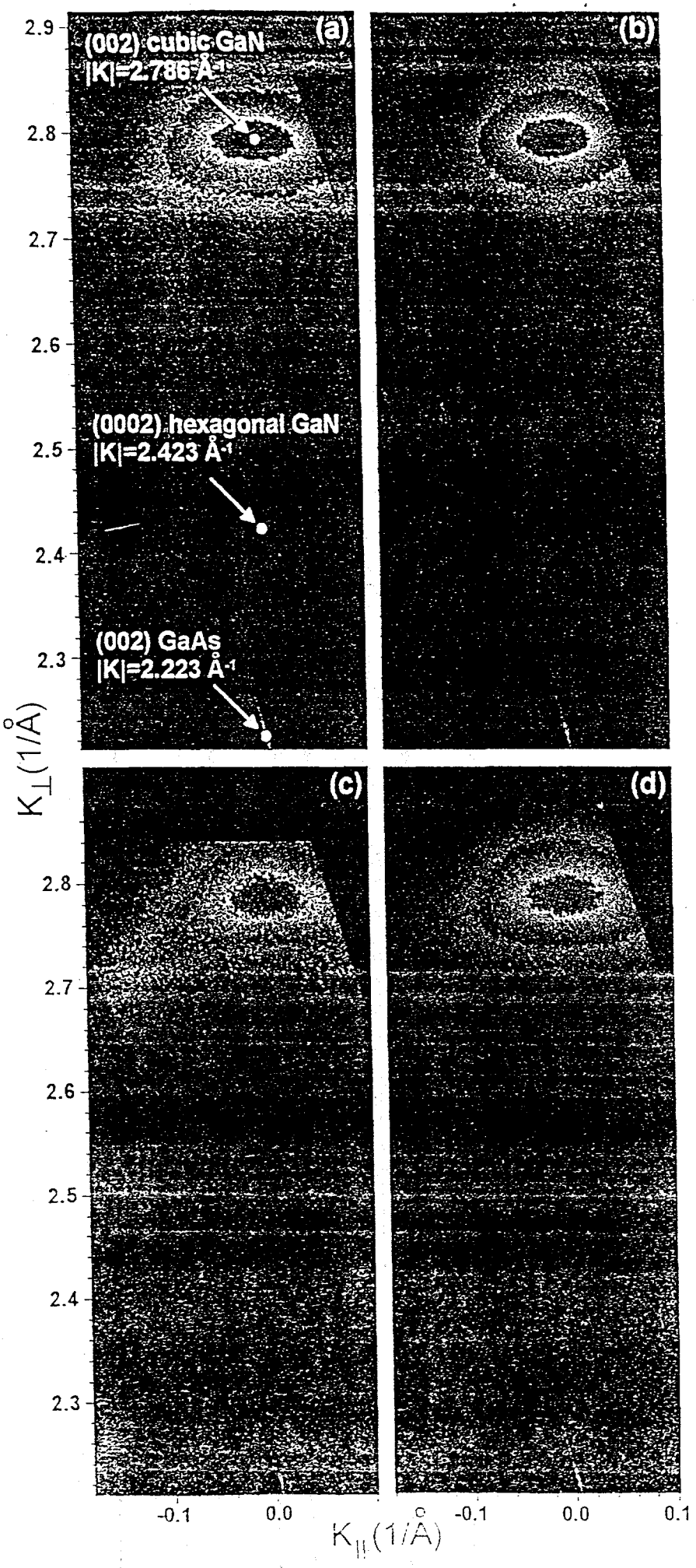
(a)
(b)
(c)
(d)
(002) cubic GaN
|K|=2.786 Å-1
(0002) hexagonal GaN
|K|=2.423 Å-1
(002) GaAs
|K|=2.223 Å-1
2.9
2.8
2.7
2.6
2.5
2.4
2.3
K⊥(1/Å)
-0.1
0.0
0.1
K||(1/Å)

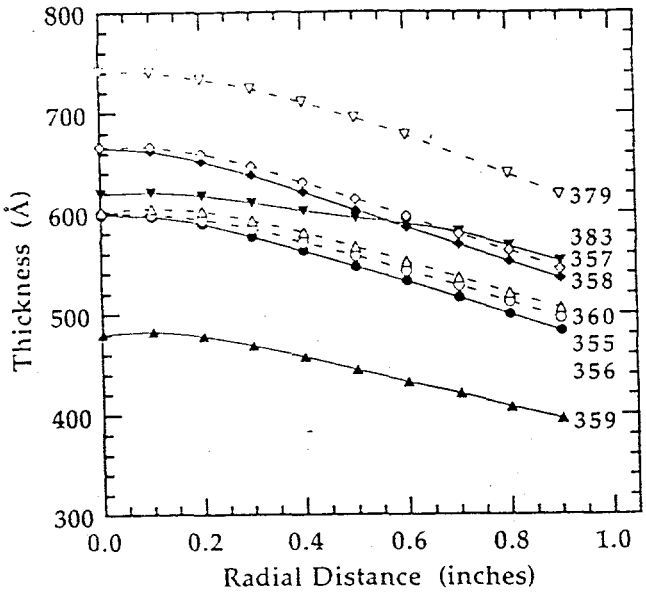
800
700
600
500
400
300
Thickness (Å)
0.0
0.2
0.4
0.6
0.8
1.0
Radial Distance (inches)
379
383
357
358
360
355
356
359

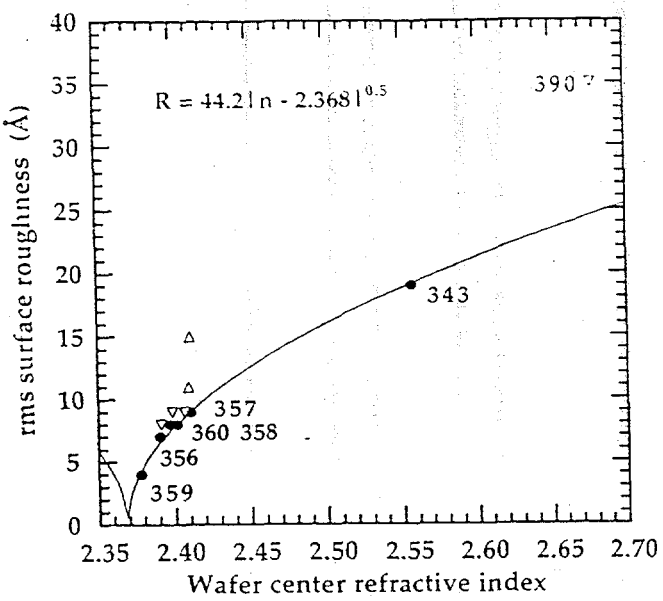
R = 44.21n - 2.3681^0.5
rms surface roughness (Å)
Wafer center refractive index
343
357
360 358
356
359
0
5
10
15
20
25
30
35
40
2.35
2.40
2.45
2.50
2.55
2.60
2.65
2.70

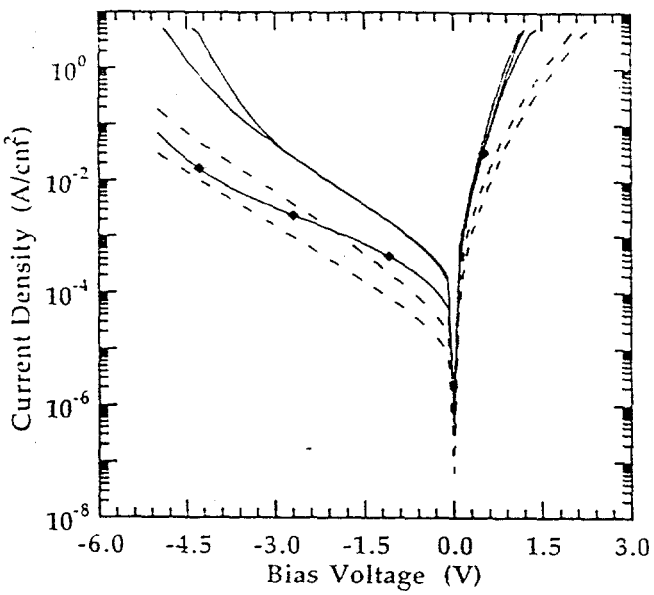
Current Density (A/cm²)
10⁰
10⁻²
10⁻⁴
10⁻⁶
10⁻⁸
-6.0
-4.5
-3.0
-1.5
0.0
1.5
3.0
Bias Voltage (V)

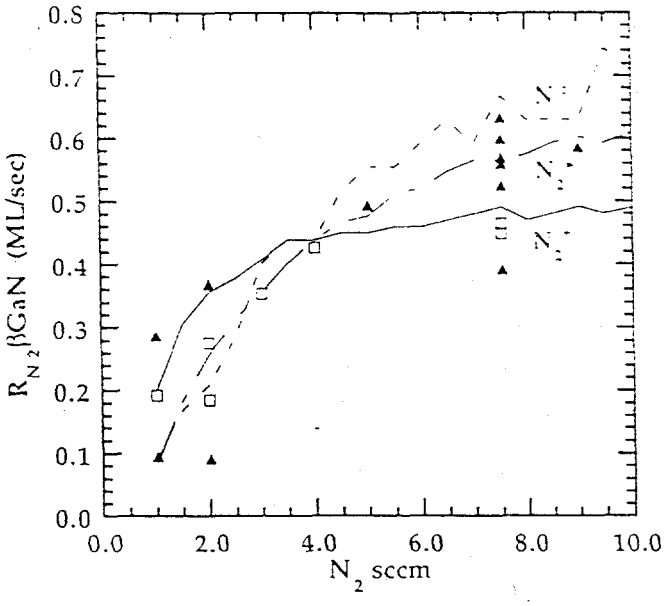
0.8
0.7
0.6
0.5
0.4
0.3
0.2
0.1
0.0
0.0
2.0
4.0
6.0
8.0
10.0
R_{N2} βGaN (ML/sec)
N_2 sccm